Journal of Alloys and Compounds 506 (2010) 804–810

Contents lists available at ScienceDirect

Journal of Alloys and Compounds

journal homepage: www.elsevier.com/locate/jallcom

One-pot synthesis of $Zn_xCd_{1-x}S$ nanocrystals with tunable optical properties from molecular precursors

Zhigang Chen[a,*], Qiwei Tian[a], Yuelin Song[a], Jianmao Yang[b], Junqing Hu[a,*]

[a] State Key Laboratory for Modification of Chemical Fibers and Polymer Materials, College of Materials Science and Engineering, Donghua University, Shanghai 201620, China
[b] Research Center for Analysis and Measurement, Donghua University, Shanghai 201620, China

ARTICLE INFO

Article history:
Received 5 April 2010
Received in revised form 8 July 2010
Accepted 8 July 2010
Available online 15 July 2010

Keywords:
Semiconductors
$Zn_xCd_{1-x}S$
Chemical synthesis
Optical property

ABSTRACT

We have reported a non-injection one-pot synthesis of the alloyed $Zn_xCd_{1-x}S$ semiconductor nanocrystals (SNCs) with controlled shapes and compositions. This non-injection approach involves heating two molecular precursors (cadmium ethylxanthate and zinc ethylxanthate) as metal and S sources in organic solvents at 320 °C for 30 min, which results in the thermal decompositions of the molecular precursors to produce $Zn_xCd_{1-x}S$. The effects of solvents and compositions on the shapes and structures of $Zn_xCd_{1-x}S$ SNCs have been investigated. The mixture solvent containing oleic acid, paraffin oil and oleylamine (such as a volume ratio: 1/2/1) results in the preparation of uniform $Zn_xCd_{1-x}S$ nanoparticles with diameters of 7–13 nm, while pure oleylamine or the mixture of oleylamine and paraffin oil as the solvent leads to the formation of uniform $Zn_xCd_{1-x}S$ nanorods. Monodisperse wurtzite $Zn_xCd_{1-x}S$ nanorods with different compositions have been prepared in pure oleylamine, and no obvious effects of the compositions on their shapes are found. Their alloying nature is consistently confirmed by the results of high-resolution transmission electron microscopy (HRTEM), X-ray diffraction (XRD) and optical measurements. These alloyed $Zn_xCd_{1-x}S$ nanorods exhibit composition-dependent absorption and emission properties, and therefore they can be promising candidates as emitting materials.

1. Introduction

Colloidal semiconductor nanocrystals (SNCs) have currently been attracting widespread scientific and technological interest due to their unique size-tunable optical and electronic properties [1–4] as well as their potential applications in solar cells [5,6], light-emitting diodes [7] and bio-labels [8–10], etc. Their small size results in the three-dimensional confinement of bulk charge carriers and the corresponding transformation from bulk energy bands to discrete 'molecular' energy states. This bulk-to-molecule transition is continuous, thus their 'band gaps' can be 'tuned' to a desired energy by controlling their particle size. The current focus on the development of their applications has increased an incentive for synthetic approaches that can offer a fastidious control over SNCs' properties. Therefore, it remains a primary objective to develop efficient routes for synthesizing high-quality and monodisperse SNCs with superior optical properties.

In the last decades, many efforts have been devoted to the preparation of binary II–VI SNCs with size-tunable optical properties [11–13]. In particular, their optical properties can be further improved by adopting a core–shell structure [13]. However, the tuning of physical and chemical properties by changing their particle size could also cause some problems (such as the instability of very small nanoparticles), which may greatly limit their applications. To address this problem, a new strategy to tune their optical properties has been developed by changing their constituent stoichiometries in mixed ternary II-II′-VI SNCs [14–21]. For these homogeneous II-II′-VI SNCs, both the confinement potential and the interfacial strain change with the composition, and therefore the energy band-gap can also be tuned with the composition even at a constant size.

A prerequisite for preparing ternary II-II′-VI SNCs is that two corresponding binary II-VI and II′-VI semiconductors should have low lattice mismatch. For example, wurtzite ZnS and CdS have *c*-axis lattice constants of 6.257 and 6.734 Å at room temperature, respectively. Such a low lattice mismatch promises the introduction of Zn^{2+} into CdS to form $Zn_xCd_{1-x}S$ alloyed SNCs. Recently, $Zn_xCd_{1-x}S$ nanoparticles [14,15], nanoflake dendrites [16], nanorods [17] and nanorod-based spherical architectures [18] have been fabricated by hydro-/solvo-thermal route. $Zn_xCd_{1-x}S$ nanorods with tunable optical properties and photocatalytic activities can be synthesized by a microwave method [19]. $Zn_xCd_{1-x}S$ nanostructured films with controllable optical properties have been prepared by dip-coating [20] and spray pyrolysis technique [21].

* Corresponding authors. Tel.: +86 21 67792975; fax: +86 21 67792855.
E-mail addresses: zgchen@dhu.edu.cn (Z. Chen), hu.junqing@dhu.edu.cn (J. Hu).

0925-8388/$ – see front matter © 2010 Elsevier B.V. All rights reserved.
doi:10.1016/j.jallcom.2010.07.075

Table 1
Effects of solvents on $Zn_xCd_{1-x}S$ SNCs[a].

Sample	Oleic acid (mL)	Paraffin oil (mL)	Oleylamine (mL)	Figure, shape
1#	10	10	0	Fig. 1a, irregular nanoparticles, $d \approx 8$–36 nm
2#	5	10	5	Fig. 1b nanoparticles, $d \approx 7$–13 nm
3#	2	16	2	Fig. 1c, nanoparticles, $d \approx 7$–13 nm
4#	0	18	2	Fig. 1d, nanorods, $d \approx 5$–10 nm, $l \approx 15$–20 nm
5#	0	10	10	Fig. 1e, nanorods, $d \approx 5$–10 nm, $l \approx 15$–35 nm
6#	0	0	20	Fig. 1f, nanorods, $d \approx 5$–10 nm, $l \approx 15$–40 nm

[a] Precursors: 1 mmol $Zn(exan)_2$ and 1 mmol $Cd(exan)_2$; thermal decomposition at 320 °C for 30 min.

One of the most predominantly employed methods for preparing SNCs involves the pyrolytic degradation of organometallic precursors in a coordinating phosphine or amine solvent [22]. In this approach, molecular complexes with pre-formed metal–chalcogen bonds act as the sources of both metal and chalcogen in the formation of these SNCs including $Zn_xCd_{1-x}S$ SNCs. For example, Li et al. [23] have prepared $Zn_xCd_{1-x}S$ SNCs with composition-dependent optical properties by a swift injection of the mixture precursors of cadmium ethylxanthate ($Cd(exan)_2$) and zinc ethylxanthate ($Zn(exan)_2$) into a hot coordinating solvent (such as the mixture of hexadecylamine and trioctylphosphine). However, hot-injection-based synthetic methods are not suitable for a large-scale production of the high-quality SNCs with narrow size distribution [24]. In order to separate the nucleation and growth stages for the fastidious size distribution, the hot-injection approach requires a fast injection of organometallic precursor solutions, a rapid decrease of the reaction temperature right after the injection, and strong stirring for efficient mass transfer; and thus the realization of these requirements is not easy at the large-scale production [24]. Accordingly, the development of the non-injection-based synthetic approaches is in demand.

In the present work, we report a non-injection one-pot synthesis of wurtzite $Zn_xCd_{1-x}S$ nanocrystals using a molecular precursor approach. This non-injection approach is easily scaled up and has great synthetic reproducibility, by heating two molecular precursors ($Cd(exan)_2$ and $Zn(exan)_2$) in an organic solvent. The effects of the solvent and composition on the shape and structure of the resulting ternary $Zn_xCd_{1-x}S$ SNCs have been investigated. In addition, their composition-dependent optical properties are also discussed.

2. Experimental details

2.1. Materials

All of the chemicals are commercially available and were used as received. Cadmium acetate dihydrate, zinc acetate dihydrate, potassium ethylxanthate, ethanol, methanol and paraffin oil were purchased from Sinopharm Chemical Reagent Co. (China). Oleic acid and oleylamine were obtained from Aldrich. Cadmium ethylxanthate ($Cd(exan)_2$) and zinc ethylxanthate ($Zn(exan)_2$) were synthesized by a method similar to that used by Nair et al. [25].

2.2. One-pot synthesis and purification

$Zn_xCd_{1-x}S$ SNCs were prepared as follows: $Zn(exan)_2$ and $Cd(exan)_2$ with total molar amount of 2 mmol and different molar ratios (10:0, 8:2, 6:4, 5:5, 4:6, 2:8, 0:10) were mixed together and dissolved in 20 mL of a solvent in a flask. The solvent was pure oleylamine or the mixture of oleylamine, oleic acid and paraffin oil with different volume ratios. The solution was slowly heated to 120 °C under vacuum with magnetic stirring for 30 min to remove residual water and oxygen during which time the flask was purged periodically with dry nitrogen gas. The resulting clear solution was then heated to 320 °C at a rate of 10 °C/min under dry nitrogen gas and kept at this temperature for 30 min. Subsequently, the mixture was allowed to cool to room temperature during which time the solution became a yellow colloidal solution. The nanocrystals were precipitated by the addition of ethanol and isolated via centrifugation at 10,000 rpm. The precipitations were then washed twice with ethanol, and further purified by dispersing in a minimum amount of chloroform and then precipitated with excess ethanol. The samples were dried under vacuum for a minimum of 24 h. The resulting nanocrystals could be dispersed in non-polar solvents (e.g. hexane, toluene, dichloromethane) by sonicating a suspension of the nanocrystals in a bath sonicator for 10–20 min.

2.3. Characterization

Sizes and morphologies of $Zn_xCd_{1-x}S$ SNCs were determined using a JEOL JEM-2010F high-resolution transmission electron microscope (HRTEM) at 200 kV. A small amount of the sample (~1 mg) was dispersed in 1 g of hexane to give an approximate 0.1 wt% solution. One drop of the resulting solution was evaporated on a formvar/carbon film supported on a copper grid. The compositions of $Zn_xCd_{1-x}S$ SNCs were measured by means of inductively coupled plasma (ICP) atomic emission using a standard HCl/HNO_3 digestion. X-ray diffraction (XRD) measurements were made with a Bruker D4 X-ray diffractometer using Cu Kα radiation ($\lambda = 0.15418$ nm). UV–vis absorption spectra were measured using a Shimadzu UV-2550 ultraviolet-visible-near-infrared spectrophotometer. Photoluminescent (PL) spectra were measured with a JASCO FP-6600 fluorescence spectrometer.

3. Results and discussion

3.1. Characterization of $Zn_xCd_{1-x}S$ SNCs prepared in different solvents

The effects of the solvents (or ligands) on the morphologies and sizes of $Zn_xCd_{1-x}S$ SNCs have been studied. Herein, $Zn_{0.5}Cd_{0.5}S$ SNCs were prepared by thermal decomposition of $Zn(exan)_2$ and $Cd(exan)_2$ with a molar ratio of 1:1 in pure oleylamine or the mixture of oleylamine, oleic acid and paraffin oil. Table 1 lists the synthetic conditions and the results. From Table 1 and Fig. 1, it is clear that the morphologies and sizes have been affected by the contents of oleic acid and oleylamine. When the solvent is the mixture of oleic acid (10 mL) and paraffin oil (10 mL) in the absence of oleylamine, only irregular nanoparticles with the size of 8–36 nm are found (Fig. 1a). With the decrease of oleic acid content (from 10 to 5 mL) and the addition of oleylamine (5 mL), SNCs are mainly monodisperse spherical particles with diameters of 7–13 nm, and they are self-assembled into an ordered array (Fig. 1b). When oleic acid content decreases to 2 mL in the presence of oleylamine (2 mL), some elongated or oblong particles are formed together with the spherical particles (Fig. 1c). Interestingly, $Zn_{0.5}Cd_{0.5}S$ SNCs prepared in the solvent without oleic acid are almost nanorods with diameters of 5–10 nm (Fig. 1d–f). With the further increase of oleylamine content, the length of the nanorods elongates. The inserted HRTEM images show well-resolved lattice fringes, demonstrating a high crystalline nature.

The effect of the solvents (or ligands) on the shapes of $Zn_xCd_{1-x}S$ SNCs should come from the difference in their coordinating ability and steric conformation, and this phenomenon is well known in the preparation of II-VI SNCs [26,27]. In this way, we can realize the shape-controllable synthesis of $Zn_xCd_{1-x}S$ SNCs by selecting appropriate solvents. For example, to synthesize uniform $Zn_xCd_{1-x}S$ nanoparticles, we use the mixture of oleic acid, paraffin oil and oleylamine (volume ratio: 1/2/1) as the solvent; to prepare uniform $Zn_xCd_{1-x}S$ nanorods, we utilize pure oleylamine (or the mixture of oleylamine and paraffin oil) as the solvent.

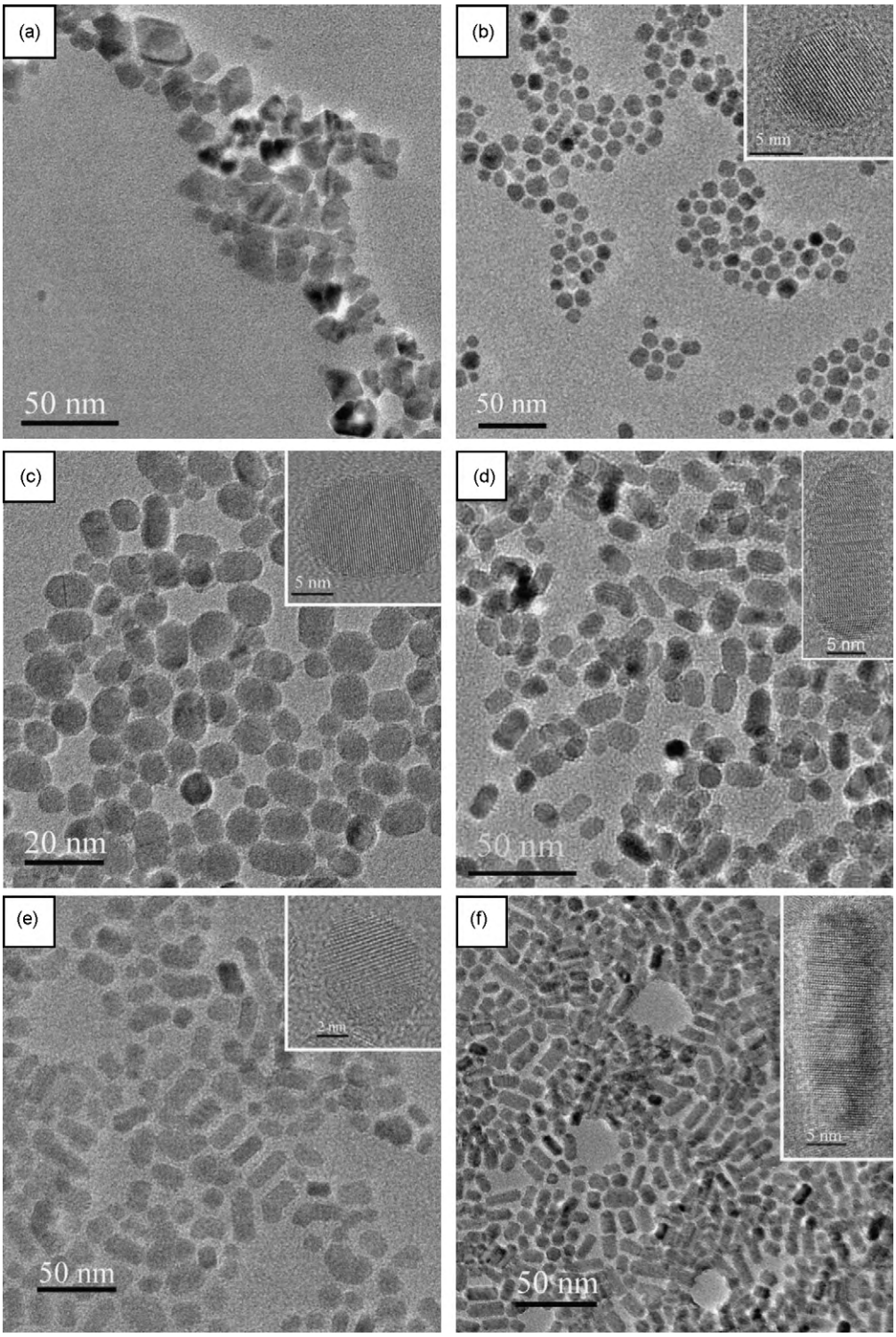

Fig. 1. TEM and HRTEM images of $Zn_xCd_{1-x}S$ SNCs used to investigate the effects of the solvents on their morphologies and sizes. All the samples were prepared under the conditions as listed in Table 1.

3.2. Characterization of $Zn_xCd_{1-x}S$ SNCs with different compositions

Subsequently, the effects of the compositions on the morphologies and structures of $Zn_xCd_{1-x}S$ SNCs have been investigated. Herein, $Zn_xCd_{1-x}S$ SNCs were prepared by thermal decomposition of $Zn(exan)_2$ and $Cd(exan)_2$ with different molar ratios in pure oleylamine at 320 °C for 30 min (see Table 2). For comparison, binary ZnS and CdS SNCs were also prepared by a similar route. In the previously reported preparation of $Zn_xCd_{1-x}S$ SNCs [24], the Zn/Cd ratio in SNCs is obviously much lower than that in the reactants, because the reaction of Cd^{2+} with S^{2-} is rapider than that of Zn^{2+} with S^{2-}. However, in our case, the Zn/Cd ratio in $Zn_xCd_{1-x}S$ SNCs is almost identical to that of $Zn(exan)_2$ to $Cd(exan)_2$, as shown in Table 2. This consistency should be attributed to the similar reaction activity and good co-dissolving property of $Zn(exan)_2$ and

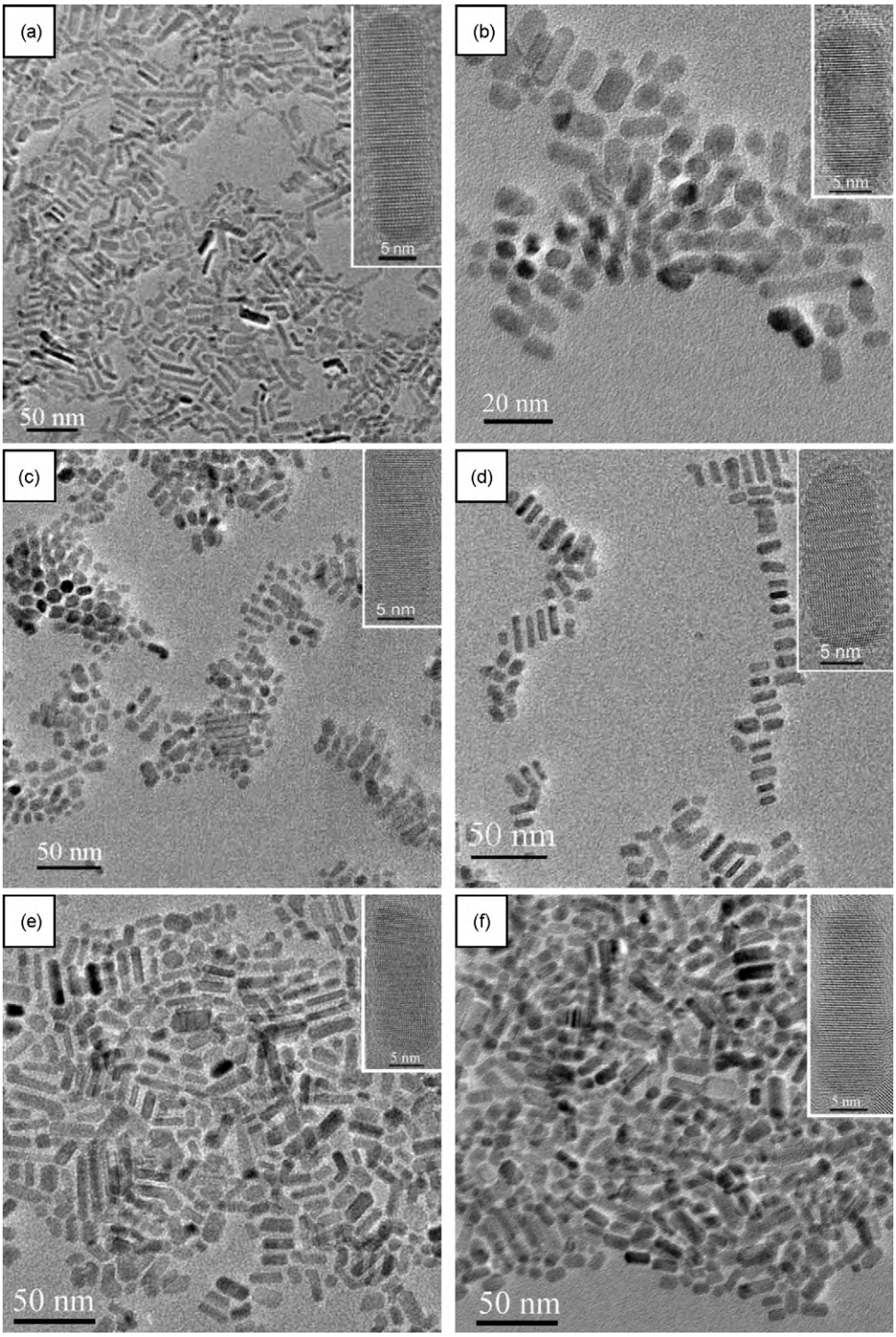

Fig. 2. TEM images of ZnS (a), $Zn_xCd_{1-x}S$ (b–e) and CdS (f) SNCs, where $Zn_xCd_{1-x}S$ SNCs were prepared at different molar ratio of $Zn(exan)_2$ to $Cd(exan)_2$: (b) 8:2, (c) 6:4, (d) 4:6, (e) 2:8. The insets are the corresponding HRTEM images.

$Cd(exan)_2$ used in the current method [23]. This fact favors the easy and accurate adjustment of the compositions of $Zn_xCd_{1-x}S$ SNCs.

Fig. 2 shows TEM and HRTEM images of ZnS, $Zn_xCd_{1-x}S$ and CdS SNCs. All of these samples are mainly nanorods with diameters of 5–10 nm and lengths of 15–40 nm. No obvious effects of the compositions on their shapes are found. This is different from the previous result about the composition-induced shape transition, in which $Zn_xCd_{1-x}S$ SNCs were prepared by swift injection of the precursors into coordinating solvents at 210 °C [23]. In their case, for ZnS, zincblende structure dominates the growth process; for CdS, it is easy to produce a zincblende 'core' at the nucleation stage and form a wurtzite arm in the following growth process. Thus, Zn/Cd molar ratio in the precursors affects the growth process and results in different shapes of the formed $Zn_xCd_{1-x}S$ SNCs. However, in our case, $Zn_xCd_{1-x}S$ SNCs were prepared by

Table 2
Effect of compositions on $Zn_xCd_{1-x}S$ SNCs[a].

Sample	Zn/Cd molar ratio in		Figure, shape
	Reactants	SNC products	
1#	10:0	–	Fig. 2a, nanorods, $d \approx 5$–10 nm, $l \approx 15$–40 nm
2#	8:2 (4.0)	3.75	Fig. 2b, nanorods, $d \approx 5$–10 nm, $l \approx 15$–40 nm
3#	6:4 (1.5)	1.46	Fig. 2c, nanorods, $d \approx 5$–10 nm, $l \approx 15$–40 nm
4#	5:5 (1.0)	0.97	Fig. 1f, nanorods, $d \approx 5$–10 nm, $l \approx 15$–40 nm
5#	4:6 (0.67)	0.66	Fig. 2d, nanorods, $d \approx 5$–10 nm, $l \approx 15$–40 nm
6#	2:8 (0.25)	0.24	Fig. 2e, nanorods, $d \approx 5$–10 nm, $l \approx 15$–40 nm
7#	0:10	–	Fig. 2f, nanorods, $d \approx 5$–10 nm, $l \approx 15$–40 nm

[a] Solvent: pure oleylamine; thermal decomposition at 320 °C for 30 min.

a non-injection one-pot synthesis at 320 °C. Since their wurtzite (hexagonal) crystal phase is thermodynamically stable, it is the favorite phase for both ZnS and CdS at high temperature process [28]. Thus, both ZnS and CdS SNCs are wurtzite nanorods (as shown in XRD pattern in Fig. 4), and Zn/Cd molar ratio in the precursors could not significantly affect the shapes of $Zn_xCd_{1-x}S$ SNCs. This fact results in the easy preparation of uniform $Zn_xCd_{1-x}S$ nanorods.

The inserted HRTEM images show well-resolved lattice fringes, demonstrating the highly crystalline nature of the nanocrystals. Furthermore, as shown in Fig. 3, the inter-planar distance of the {0 0 2} plane goes up linearly (from 3.11 Å for ZnS to 3.18 Å for $Zn_{0.8}Cd_{0.2}S$, and 3.21 Å for $Zn_{0.6}Cd_{0.4}S$, then to 3.36 Å for CdS), with the increase of Cd content. These results indicate that *c*-axis of $Zn_xCd_{1-x}S$ SNCs extends with the increase of Cd molar fraction, which is an evidence for the formation of the ternary alloyed SNCs.

Powder XRD patterns reveal a hexagonal wurtzite structure of SNCs over all compositions (Fig. 4). No phase-structure change is observed, which is one of key reasons for no composition-induced shape transition in our case and is different from the previous XRD results [23]. The characteristic XRD patterns of SNCs exhibit seven prominent peaks, which are indexed to the scattering from (1 0 0), (0 0 2), (1 0 1), (1 0 2), (1 1 0), (1 0 3), and (1 1 2) planes, respectively. XRD peaks also shift to smaller angle gradually as Cd content increases. This continuous peak-shift of $Zn_xCd_{1-x}S$ SNCs may also rule out phase separation and/or separated nucleation of CdS or ZnS nanocrystals. As shown in Fig. 5, the lattice parameter *c* of $Zn_xCd_{1-x}S$ SNCs measured from XRD patterns goes up nearly linearly as Cd content increases, which agrees with the data measured from HRTEM images (Figs. 2 and 3). This trend is also consistent with Vegard's law and indicates a homogeneous alloy structure [29–31].

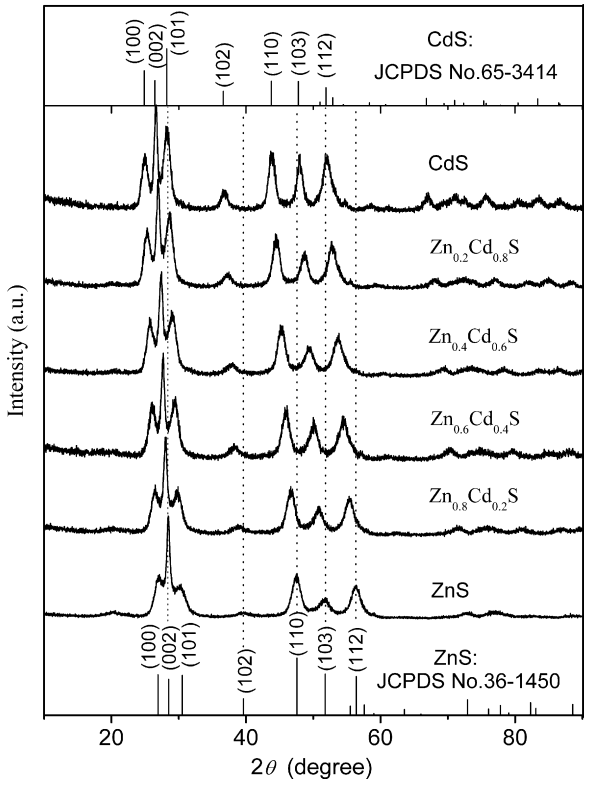

Fig. 4. Power XRD patterns of ZnS, $Zn_xCd_{1-x}S$ and CdS SNCs. The standard patterns of wurtzite phase of ZnS (JCPDS card no. 36-1450) and CdS (JCPDS card no. 65-3414) are also supplied.

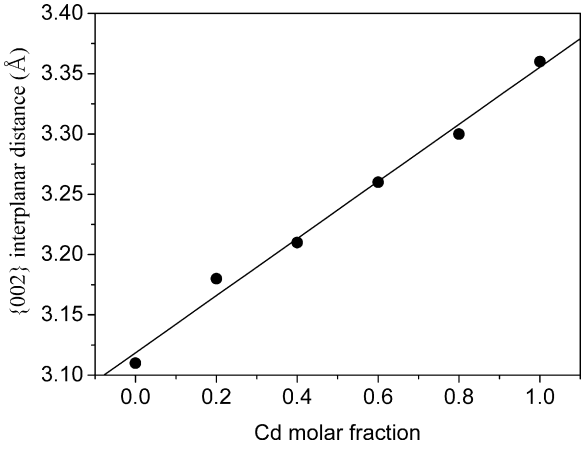

Fig. 3. The {0 0 2} inter-planar distances measured from the inserted HRTEM images in Fig. 2 as a function of Cd molar fraction.

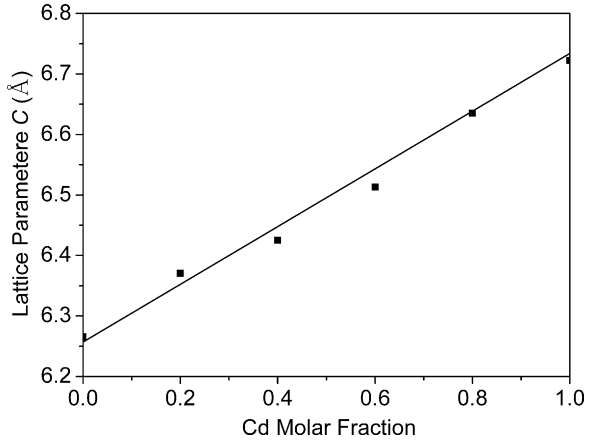

Fig. 5. A linear relationship of the lattice parameter *c* of ZnS, $Zn_xCd_{1-x}S$ and CdS SNCs as a function of Cd molar fraction, which is measured from XRD patterns (square data points) and calculated from Vegard's law (solid line).

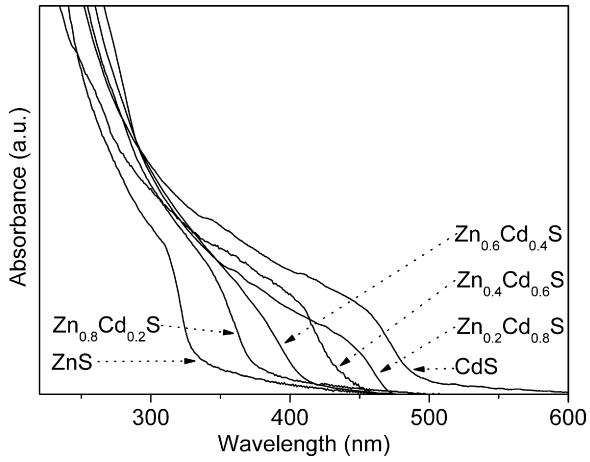

Fig. 6. UV–vis absorption spectra of ZnS, $Zn_xCd_{1-x}S$ and CdS SNCs.

3.3. Optical properties of $Zn_xCd_{1-x}S$ SNCs

The absorption spectra of ZnS, $Zn_xCd_{1-x}S$ and CdS SNCs prepared in pure oleylamine are shown in Fig. 6. Typical ZnS SNCs exhibit an absorption edge at about 330 nm. As Zn content (x value) in SNCs decreases from 1 to 0.2, the absorption edge of $Zn_xCd_{1-x}S$ SNCs gradually shifts from 330 to 472 nm, and ultimately CdS SNCs have an absorption edge at about 490 nm. It has been revealed that SNCs with a radius significantly smaller than the exciton Bohr radius show strong size-dependent optical properties due to the strong quantum confinement effect of the charge carriers [23,24]. A weak quantum confinement effect occurs when the particle radius is close to or somewhat larger than the Bohr radius. ZnS and CdS have typical exciton Bohr radii of 2.2 and 3.0 nm, respectively. In our case, $Zn_xCd_{1-x}S$ SNCs are actually in the weak quantum confinement regime because their radii are larger than those of Bohr radii. Thus, such a large shift in the absorption edge cannot be attributed to the quantum-size effect, but should be related to a continuous change in the energy band-gap (E_g) of $Zn_xCd_{1-x}S$ SNCs with different Zn/Cd ratio [23].

For a direct band-gap material, the absorption coefficient satisfies the equation $(\alpha h\nu)^2 = A(h\nu - E_g)$. The band-gap ($E_g$) values of $Zn_xCd_{1-x}S$ SNCs were obtained by extrapolation of the plot of $(\alpha h\nu)^2$ vs. $(h\nu)$, as shown in Fig. 7a. With the decrease of Zn content (x value) in $Zn_xCd_{1-x}S$ SNCs from 1 to 0, E_g went down from 3.75 eV for ZnS SNCs to 2.54 eV for CdS SNCs. As demonstrated in Fig. 7b, these results can be well fitted by the empirical relationship for bulk $Zn_xCd_{1-x}S$: $E_g(x) = 2.5 + 0.59x + 0.61x^2$; where the quantum-size confinement effect is not obvious [23].

Fig. 8 shows the corresponding PL spectra of $Zn_xCd_{1-x}S$ SNCs. The PL spectra display only symmetric and narrow band-gap-emission peaks, and the peak shifts systematically from 382 to 475 nm with the increase of Cd molar fraction from 0.2 to 0.8 in $Zn_xCd_{1-x}S$ SNCs (x = 0.8, 0.6, 0.4, 0.2). On the one hand, this sole emission peak in PL spectra reveals that surface-defect emission is suppressed [23]. On the other hand, this significant red-shift provides a clear evidence for the formation of the band-gap of the alloyed $Zn_xCd_{1-x}S$ SNCs via intermixing the wider band-gap of ZnS (3.7 eV) with the narrower band-gap of CdS (2.5 eV).

It is well known that the corresponding absorption and PL peaks of CdS and ZnS nanocrystals should appear respectively if CdS or ZnS nucleates separately [23]. In our case, the sole absorption and PL peaks of the resulting $Zn_xCd_{1-x}S$ SNCs rule out the separate nucleation of CdS and ZnS, which agree with the results of HRTEM and XRD characterizations. If a core–shell structure is formed, such a significant shift of the optical spectra cannot be produced compared with those of the core materials. Therefore, our $Zn_xCd_{1-x}S$ SNCs exhibit excellent composition-dependent optical properties.

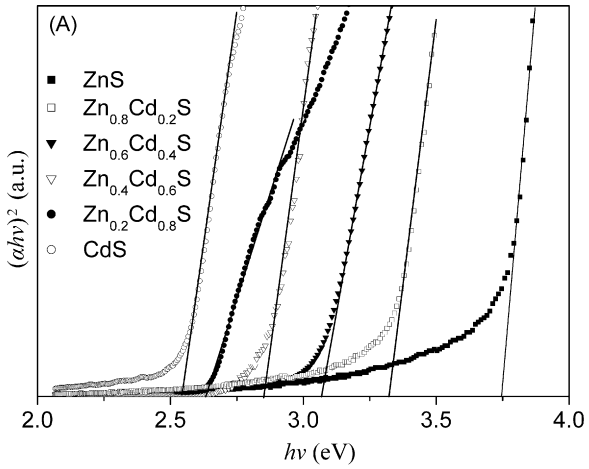

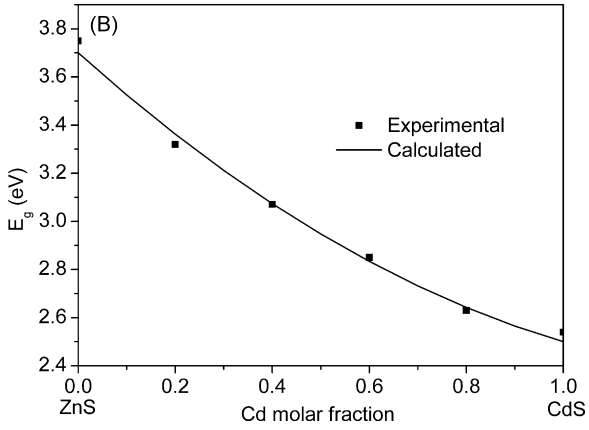

Fig. 7. (a) The variation of $(\alpha h\nu)^2$ as a function of photon energy ($h\nu$) for $Zn_xCd_{1-x}S$ SNCs; (b) band-gap (E_g) as a function of Cd molar fraction for $Zn_xCd_{1-x}S$ SNCs (square data points, obtained by extrapolation of the plot of $(\alpha h\nu)^2$ vs. ($h\nu$)) and bulk $Zn_xCd_{1-x}S$ (solid line, calculated from the empirical relationship).

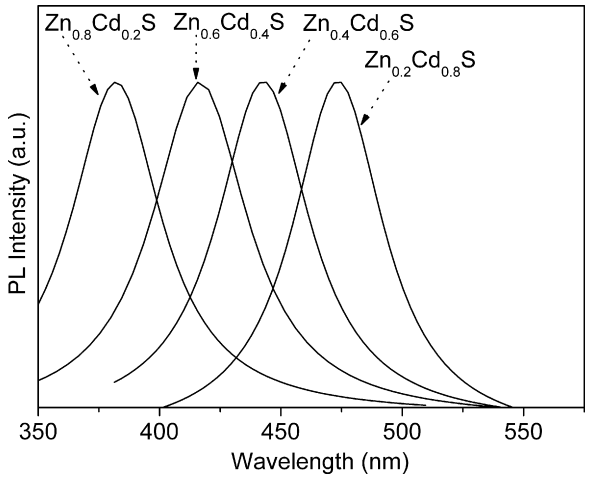

Fig. 8. PL spectra of $Zn_xCd_{1-x}S$ SNCs.

4. Conclusions

$Zn_xCd_{1-x}S$ SNCs have been prepared by a non-injection one-pot synthesis approach consisting of thermal decomposition of $Zn(exan)_2$ and $Cd(exan)_2$ in pure oleylamine or the mixture of

oleylamine, oleic acid and paraffin oil. The shape-controllable synthesis of $Zn_xCd_{1-x}S$ SNCs is realized by selecting the appropriate solvents. When pure oleylamine is used as the solvent, no obvious composition-induced shape transition is found, and $Zn_xCd_{1-x}S$ SNCs with different compositions are mainly wurtzite nanorods with diameters of 5–10 nm and lengths of 15–40 nm. With the increase of Cd content, both the lattice parameter and energy bandgap of $Zn_xCd_{1-x}S$ SNCs go up gradually. These alloyed $Zn_xCd_{1-x}S$ nanorods exhibit excellent composition-dependent optical properties and are promising candidates as emitting materials.

Acknowledgements

This work was financially supported by the Program for New Century Excellent Talents of the University in China, the National Natural Science Foundation of China (Grant No. 50872020 and 50902021), the "Pujiang" Program of Shanghai Education Commission in China (Grant No. 09PJ1400500), the "Dawn" Program of Shanghai Education Commission in China (Grant No. 08SG32), Specialized Research Fund for the Doctoral Program of Higher Education (Grant No. 20090075120014), "Chen Guang" project (Grant No. 09CG27) supported by Shanghai Municipal Education Commission and Shanghai Education Development Foundation, the Fundamental Research Funds for the Central Universities, and the Program of Introducing Talents of Discipline to Universities (Grant No. 111-2-04).

References

[1] A.F.G. Monte, D. Rabelo, P.C. Morais, J. Alloys Compd. 495 (2010) 436.
[2] P. Chawla, S.P. Lochab, N. Singh, J. Alloys Compd. 492 (2010) 662.
[3] C.B. Murray, C.R. Kagan, M.G. Bawendi, Annu. Rev. Mater. Sci. 30 (2000) 545.
[4] A.L. Efros, M. Rosen, Annu. Rev. Mater. Sci. 30 (2000) 475.
[5] Z.J. Cheng, F.F. Su, L.K. Pan, M.L. Cao, Z. Sun, J. Alloys Compd. 494 (2010) L7.
[6] I. Robel, V. Subramanian, M. Kuno, P.V. Kamat, J. Am. Chem. Soc. 128 (2006) 2385.
[7] S. Coe, W.K. Woo, M. Bawendi, V. Bulovic, Nature 420 (2002) 800.
[8] M. Bruchez, M. Moronne, P. Gin, S. Weiss, A.P. Alivisatos, Science 281 (1998) 2013.
[9] W.C. Chan, S.M. Nie, Science 281 (1998) 2016.
[10] J.K. Jaiswal, H. Mattoussi, J.M. Mauro, S.M. Simon, Nat. Biotechnol. 21 (2003) 47.
[11] M. Romcevic, N. Romcevic, R. Kostic, L. Klopotowski, W.D. Dobrowolski, J. Kossut, M.I. Comor, J. Alloys Compd. 497 (2010) 46.
[12] Z.A. Peng, X.G. Peng, J. Am. Chem. Soc. 123 (2001) 183.
[13] B. Mahler, N. Lequeux, B. Dubertret, J. Am. Chem. Soc. 132 (2010) 953.
[14] S.N. Zu, Z.Y. Wang, B. Liu, X.P. Fan, G.D. Qian, J. Alloys Compd. 476 (2009) 689.
[15] S.Y. Li, Y. Jiang, M. Niu, C. Wang, J.S. Jie, J. Alloys Compd. 481 (2009) 644.
[16] W. Yu, P.F. Fang, S.J. Wang, J. Alloys Compd. 486 (2009) 780.
[17] L.Z. Wang, Y. Jiang, C. Wang, W.H. Wang, B.L. Cao, M. Niu, Y.T. Qian, J. Alloys Compd. 454 (2008) 255.
[18] Y.Q. Chen, X.H. Zhang, C. Jia, Y. Su, Q. Li, J. Phys. Chem. C 113 (2009) 2263.
[19] W.J. Li, D.Z. Li, W.J. Zhang, Y. Hu, Y.H. He, X.Z. Fu, J. Phys. Chem. C 114 (2010) 2154.
[20] M. Abdel Rafea, A.A.M. Farag, N. Roushdy, J. Alloys Compd. 485 (2009) 660.
[21] Y. Raviprakash, K.V. Bangera, G.K. Shivakumar, Curr. Appl. Phys. 10 (2010) 193.
[22] Z.A. Peng, X.G. Peng, J. Am. Chem. Soc. 123 (2001) 1389.
[23] Y.C. Li, M.F. Ye, C.H. Yang, X.H. Li, Y.F. Li, Adv. Funct. Mater. 15 (2005) 433.
[24] J.Y. Ouyang, C.I. Ratcliffe, D. Kingston, B. Wilkinson, J. Kuijper, X.H. Wu, J.A. Ripmeester, K. Yu, J. Phys. Chem. C 112 (2008) 4908.
[25] P.S. Nair, T. Radhakrishnan, N. Revaprasadu, G. Kolawole, P. O'Brien, J. Mater. Chem. 12 (2002) 2722.
[26] N. Pradhan, B. Katz, S. Efrima, J. Phys. Chem. B 107 (2003) 13843.
[27] Y.C. Li, X.H. Li, C.H. Yang, Y.F. Li, J. Phys. Chem. B 108 (2004) 16002.
[28] T. Vossmeyer, G. Reck, L. Katsikas, E.T.K. Haupt, B. Schulz, H. Weller, Science 267 (1995) 1476.
[29] L. Vegard, H. Schjelderup, Phys. Z 18 (1917) 93.
[30] J.K. Furdyna, J. Appl. Phys. 64 (1988) R29.
[31] W.Z. Wang, W. Zhu, H.L. Xu, J. Phys. Chem. C 112 (2008) 16754.